Self-Assembly and Chemical Modifications of Bisphenol A on Cu(111): Interplay Between Ordering and Thermally Activated Stepwise Deprotonation

ARTICLE *in* ACS NANO · DECEMBER 2013

Impact Factor: 12.88 · DOI: 10.1021/nn4030493 · Source: PubMed

Self-Assembly and Chemical Modifications of Bisphenol A on Cu(111): Interplay Between Ordering and Thermally Activated Stepwise Deprotonation

Sybille Fischer,[†] Anthoula C. Papageorgiou,[†] Julian A. Lloyd,[†] Seung Cheol Oh,[†] Katharina Diller,[†] Francesco Allegretti,[†] Florian Klappenberger,[†] Ari Paavo Seitsonen,[‡] Joachim Reichert,[†,*] and Johannes V. Barth[†]

[†]Physik Department E20, Technische Universität München, D-85748 Garching, Germany and [‡]Physikalisch-Chemisches Institut der Universität Zürich, Winterthurerstrasse 190, CH-8057 Zürich, Switzerland

ABSTRACT Bisphenol A (BPA) is a chemical widely used in the synthesis pathway of polycarbonates for the production of many daily used products. Besides other adverse health effects, medical studies have shown that BPA can cause DNA hypomethylation and therefore alters the epigenetic code. In the present work, the reactivity and self-assembly of the molecule was investigated under ultra-high-vacuum conditions on a Cu(111) surface. We show that the surface-confined molecule goes through a series of thermally activated chemical transitions. Scanning tunneling microscopy investigations showed multiple distinct molecular arrangements dependent on the temperature treatment and the formation of polymer-like molecular strings for temperatures above 470 K. X-ray photoelectron spectroscopy measurements revealed the stepwise deprotonation of the hydroxy groups, which allows the molecules to interact strongly with the underlying substrate as well as their neighboring molecules and therefore drive the organization into distinct structural arrangements. On the basis of the combined experimental evidence in conjunction with density functional theory calculations, structural models for the self-assemblies after the thermal treatment were elaborated.

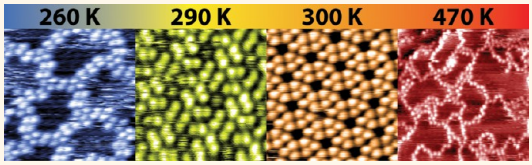

KEYWORDS: bisphenol A · copper surface · self-assembly · deprotonation · scanning tunneling microscopy · X-ray photoelectron spectroscopy · near-edge X-ray absorption fine structure · density functional theory

Bisphenol A (BPA, systematic name: 4,4′-(propane-2,2-diyl)diphenol, Figure 1a) is a chemical commonly employed in polymerization reactions, *e.g.*, for the fabrication of polycarbonates widely used in products such as optical media, lenses, and bottles. The high exposure to humans due to its use in plastics for food and beverage packaging has brought this chemical into the public eye. It has been shown to be a hormone mimic, and as an artificial estrogen it is linked to infertility[1] and other health hazards.[2] Additionally, BPA is under suspicion of interfering with DNA methylation processes,[3,4] a natural procedure for activation and silencing of certain genes playing a pronounced role in DNA error correction. In nature, DNA methylation is performed by methyl-transferase proteins, but environmental influences such as chemicals have also been reported to trigger or suppress the methylation processes and thus altering the so-called epigenetic code. However, at present, there is a lack of mechanistic insight of the molecular events and the role of the BPA functional moieties in this process. To aid the comprehension of such effects in a complex biological environment, it is of interest to develop a detailed understanding of the molecule's behavior and reactivity at well-defined conditions, herein provided by an atomistically clean metal surface lattice under ultra-high-vacuum (UHV) conditions. Previous studies of molecules of biological importance adsorbed on metal surfaces have shown that the intermolecular interactions are very sensitive to changes in the chemical state of the molecules and are manifested by metamorphoses of the molecular self-assembly.[5−8] The reactivity of specific functional groups and the activation of certain reactive groups in a precise manner can alter

* Address correspondence to joachim.reichert@tum.de.

Received for review June 17, 2013 and accepted December 5, 2013.

Published online December 16, 2013
10.1021/nn4030493

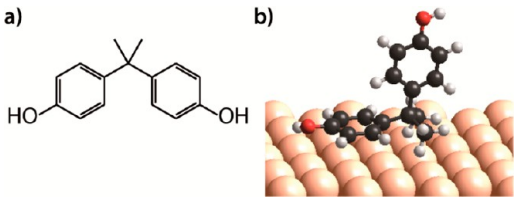

Figure 1. Bisphenol A: (a) molecular structure and (b) DFT model of an adsorption geometry on Cu(111) with one phenol unit pointing away from the substrate. C, O, H, and Cu atoms are shown in black, red, white, and orange, respectively.

the balance of intermolecular interactions, which in turn enables certain reaction outcomes. In this context, the stable functionalization of a surface with BPA molecules might offer a precise trigger for controlling the methylation processes of DNA bases and their derivates. Hitherto the studies of the BPA reactivity have focused on the biological,[3,4] chemical,[9,10] and technological[11−14] properties of BPA as a polymerization component and the widespread related polymer BPA polycarbonate.

Here we present a comprehensive study of the temperature-dependent self-assembly and chemical behavior of BPA adsorbed on Cu(111). The copper template, which is offering a well-defined atomically flat surface, was used as a catalytically active substrate with the ability to anchor molecules so as to allow formation of high-temperature phases. Scanning tunneling microscopy (STM) has proven to be a valuable tool for the study of polymorphism and molecular self-assembly of numerous organic molecules, including drugs and nonplanar molecules.[15−18] X-ray spectroscopy techniques are suitable for monitoring changes in the chemical state and spatial orientation of the molecules.[5,6,19−22] With STM we observed four irreversible transformations into five distinct molecular assemblies as a function of the sample annealing temperature. High-resolution X-ray photoelectron spectroscopy (XPS) measurements were employed to shed light on the chemical state of the molecules and to correlate it to the STM data. Angle-resolved near-edge X-ray absorption spectroscopy (NEXAFS) provided information concerning the orientation of the molecules' aromatic rings with respect to the surface. On the basis of the combined experimental evidence in conjunction with density functional theory (DFT) calculations, structural models for the self-assembly after the thermal treatment were elaborated.

RESULTS AND DISCUSSION

Self-Assembly as a Function of Thermal Treatment. Upon deposition (*cf.* Methods) onto a Cu(111) sample held at ∼260 K (Figure 2a), the BPA molecules assemble into an irregular open porous network (henceforth referred to as "network-phase"), which consists of interconnected filaments built by BPA molecules.

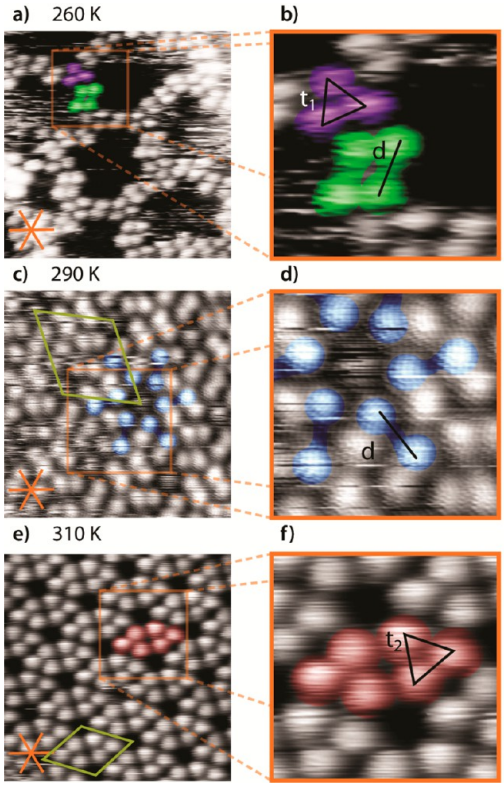

Figure 2. STM images of different structures of BPA on Cu(111). The Cu(111) high-symmetry axes are indicated in orange in images (a), (c), and (e). (a) Network-phase, observed upon BPA deposition at a sample temperature of ∼260 K (13.2 × 13.2 nm^2, I_t = 120 pA, U_t = 1.5 V) with a trimer and two dimer motifs highlighted in purple and green, respectively. (b) Magnification (4.4 × 4.4 nm^2) of the area indicated in (a) with the intermolecular spacings t_1 and d annotated. (c) Dimer-phase observed after warming the network-phase to 290 K (9.7 × 9.7 nm^2, I_t = 80 pA, U_t = 2.2 V). The (*S*)-mill and the unit cell are marked in blue and green, respectively. (d) Magnification (4.4 × 4.4 nm^2) of the area indicated in (c) with d marking the spacing of the dimer. (e) Trimer-phase observed after annealing the dimer-phase to 300−340 K (11.4 × 11.4 nm^2, I_t = 90 pA, U_t = 2.5 V). Two facing trimers and the unit cell are indicated in red and green, respectively. (f) Magnification (4.4 × 4.4 nm^2) of the area indicated in (e), with t_2 marking the molecule to molecule distance within the trimer.

The filament-like sections in this phase are composed of an even number of distinct protrusions paired together in the STM image (highlighted in green in Figure 2a,b), whereas the nodes comprise three protrusions of similar appearance (purple in Figure 2a,b). The coexistence of dimers and trimers excludes the possibility that the bright protrusions are associated with submolecular features, whence we conclude that each bright protrusion corresponds to an integral number of molecular units. Taking into account the typical lateral separation among adjacent bright protrusions, these can only correspond to individual molecules. Warming the sample to ∼290 K (room temperature) results into a structure consisting purely of dimers ("dimer-phase"), which assemble into chiral mill-like structures (a motif is highlighted in blue in

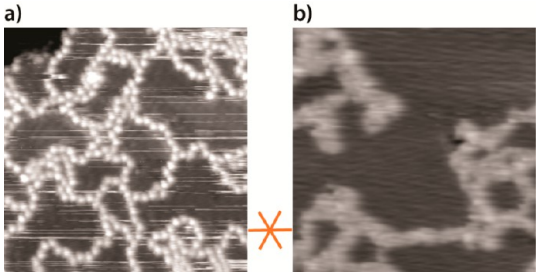

Figure 3. STM micrographs of the molecular chains. (a) Type A: After annealing the sample to 470−570 K (23 × 23 nm^2, I_t = 120 pA, U_t = 1.77 V) distinct protrusions can be distinguished in STM images. (b) Type B: These features were smeared out after annealing to ∼700 K (23 × 23 nm^2, I_t = 120 pA, U_t = 1.25 V) and the chains on the surface appear less defined. The high-symmetry axes of the Cu(111) substrate are indicated in orange.

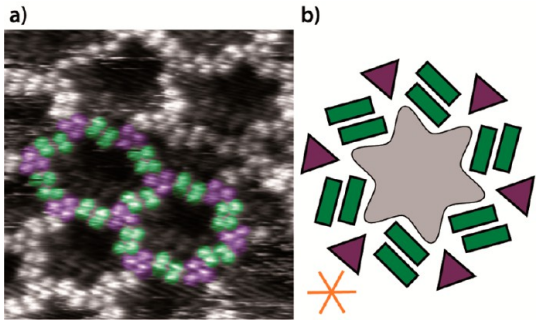

Figure 4. Star-shaped pores (a) observed in the network-phase (17.6 × 17.6 nm^2, I_t = 130 pA, U_t = 1.5 V) and highlighted in color along with (b) a schematic model of this arrangement. The purple triangles and green rectangles represent the trimers and dimers, respectively. The high-symmetry axes of the Cu(111) substrate are indicated in orange.

Figure 2c) constituting a two-dimensional supramolecular network. Further annealing to temperatures between 300 and 340 K causes the BPA layer to change into a structure built up only from trimers ("trimer-phase", Figure 2e). The dimer- and trimer-phases feature a long-range-ordered structure and extend almost free of defects over large areas (∼ 50 × 50 nm^2) of the sample. Following annealing of the crystal to 470 K, a new structure consisting of meandering chains with identifiable molecular features appears. Figure 3a displays a typical STM image of this phase ("molecular chains of type A"), which is stable up to a temperature of 570 K. For higher annealing temperatures, the boundaries between individual molecular features start to blur, until no protrusions are distinguishable within the chains for T > 700 K ("molecular chains of type B", Figure 3b).

As mentioned above, the network-phase consists of filaments composed by dimers that are connected by trimeric motifs (Figure 2a). These dimers are characterized by monomers with a spacing of d = 11 ± 1 Å, which pair along the ⟨1$\bar{1}$0⟩ directions of the underlying copper substrate. The trimer molecules have a distance of t_1 = 9.1 ± 1.0 Å with respect to each other with t_1 running close to the ⟨$\bar{1}$12⟩ Cu(111) directions (Figure 2b). The pore size within the molecular network varies appreciably between values of 3 to 22 nm^2, although ∼40% of these pores form a distinct star-like motif with a measured pore size of 15−20 nm^2. These six-pointed star-shaped pores consist of six dimer pairs, connected by trimers (Figure 4). The differences in the pore size and shape originate from small variations of this assembly, such as an additional or missing dimer or a different orientation of one of the dimer pairs. Within the pores, streaks indicate diffusing molecules on the surface imaged at 180 K.

The dimer-phase forming after heating the sample to 290 K consists of six dimers arranged in a mill-like structure. Although BPA is an achiral molecule, chirality is expressed in its self-assembly in the dimer-phase. This organizational chirality is hierarchically transferred from the formation of dimers, similar to multilevel chiral structure formations in rubrene assemblies[23] and metallosupramolecular nanoporous layers.[24] In some of the centers of the mill structure one can discern a protrusion of fuzzy appearance representing a trapped molecule, whose diffusion is constrained by the surrounding dimers. The spacing between the molecules within the dimer is also d ≈ 11 Å along the Cu(111) high-symmetry directions (Figure 2d). The molecular superstructure can be described by a hexagonal unit cell with a side length of a = 3.5 ± 0.2 nm, rotated by ∼12° with respect to the copper ⟨1$\bar{1}$0⟩ directions (Figure 2c). Notably, extended molecular domains of both chiral mills (cf. Figure S1a) were identified in our STM study with the two-dimensional islands consisting solely of either (*R*)- or (*S*)-mills without any chiral defects.

Similarly to the dimer-phase, in the trimer-phase the molecules assemble in a highly ordered arrangement with a unit cell side length of a = 2.7 ± 0.1 nm and the axes rotated by ∼14° with respect to the Cu ⟨1$\bar{1}$0⟩ directions (Figure 2e). The spacing of the individual molecules in the trimer is t_2 = 9.7 ± 0.5 Å (Figure 2f). Rotation of the overlayer unit cell with respect to the substrate gives rise to six symmetrically equivalent domains (Figure S1b).

Annealing to temperatures between 470 and 570 K results in a random chain structure (type A) composed of individual molecules linked together (Figure 3a), at variance with the described network-phase, where the filaments are formed from BPA dimers. The molecule to molecule distance is ∼9.6 Å. Following annealing to 570 K, the individual features of the molecular structure start to smear out. Further annealing to 700 K results in the loss of distinct features within the chains (type B), which appear broader and more contracted (Figure 3b). Concomitantly, the chain distribution becomes more irregular and the apparent height decreases by ∼0.4 Å. It is noteworthy that while the

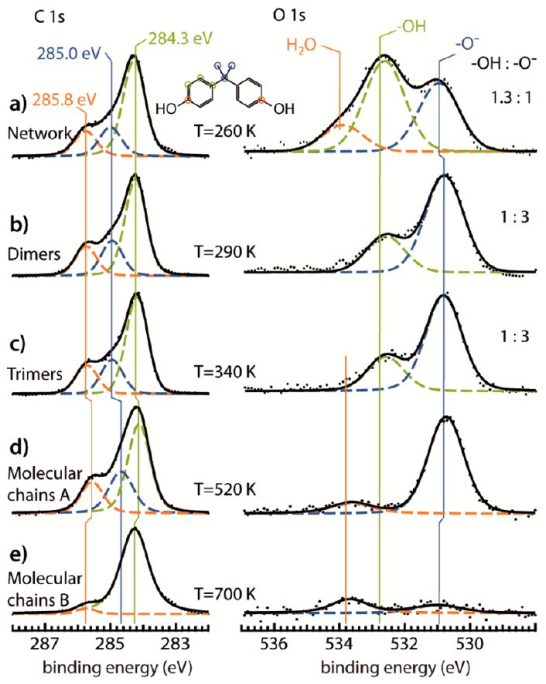

Figure 5. High-resolution X-ray photoelectron spectra and fitting of the C 1s (left) and O 1s (right) core levels corresponding to (a) the network-phase, (b) the dimer-phase, (c) the trimer-phase, (d) the molecular chains type A, and (e) the molecular chains type B of submonolayer BPA adsorbed on the Cu(111) surface. The annealing temperature used for the formation of these phases is indicated between the spectra, and the −OH to $-O^-$ ratios are shown on the right.

dimer-phase and the trimer-phase exhibit significant surface mobility at room temperature, STM data of the chain structures at the same temperature reveal much higher stability, which is typical for strong intermolecular linking and/or a strong molecule−substrate interaction. Interestingly, this series of irreversible structural transitions could not be observed on the more inert Ag(111) surface, pointing to a decisive role of the molecule−substrate interaction.

Chemical State and Molecular Orientation as a Function of Thermal Treatment. In order to examine the driving force of these changes in the structure of the molecular assembly, additional synchrotron-based XPS and NEXAFS experiments were performed. While the C 1s spectrum of BPA adsorbed on Cu(111) does not change as a function of the annealing temperature from 260 to 520 K (see Figure 5, left), the O 1s spectra are significantly affected by the thermal treatment. The C 1s spectrum shows three signals at binding energies of 284.3, 285.0, and 285.8 eV, which can be attributed to the contributions of aromatic, aliphatic, and hydroxy-related aromatic carbon atoms, respectively.[11] The O 1s spectrum of the network-phase can be fitted with three peaks (Figure 5a, right). The signals at binding energies of 532.7 and 531.1 eV can be assigned to the oxygen of phenol (Ph−OH) and phenolate (Ph−O^-) groups, respectively.[25,26] BPA can act as a weak acid (pK_A = 9.8)[27] and has a higher probability of hydroxyl group deprotonation than for example ethanol (pK_A = 16), because the resulting species is stabilized *via* the aromatic ring. A third signal appearing as a high-energy shoulder of the O 1s spectrum at a binding energy of 534.0 eV is attributed to H_2O, originating from the residual gases in the vacuum sticking to Cu(111) during preparations at 140 K.[28] The alternative scenario of CO as a possible contaminant can be ruled out, based on the cleanness of the C 1s signal.[29] The ratio of the relative intensities of the −OH:−O^- group signals is ∼1.3:1. This ratio indicates that approximately half of the BPA phenols in the dimer-phase deprotonate upon adsorption at ∼260 K, a deprotonation which also occurs for phenol adsorbed on the Cu(110) surface.[30]

Warming to 290 K and higher temperatures leads to a decrease of the phenol signal intensity at 532.7 eV and a concomitant increase of the phenolate signal at a binding energy of 530.9 eV (Figure 5b, right), in a ratio of 1:3. The high-energy shoulder disappears, supporting its earlier assignment to H_2O. The −OH signal has exactly the same binding energy in all three phases, whereas the $-O^-$ signal shifts by 0.2 eV to lower binding energies at ∼290 K, which is the temperature marking the transition from the network-phase to the dimer-phase. This shift is tentatively ascribed to a difference in the local environment of the deprotonated groups resulting from increased intermolecular interactions in the more dense phases.

Thermal treatment of the BPA overlayer to 340 K (Figure 5c, right) leaves the XPS signatures virtually unaffected. This indicates that no chemical transformation drives the structural change from the dimer-phase to the trimer-phase; that is, these two phases are two-dimensional crystal polymorphs of the same constituents. Considering the higher formation temperature of the trimer-phase, the temperature of ∼300 K might be needed to form the energetically more stable trimeric arrangement.

The molecular chains of type A appearing after high-temperature (470−570 K) treatment (Figure 5d, right) no longer retain any protons in the alcohol moieties. The O 1s spectrum shows only the phenolate contribution at 530.9 eV and a new weak signal at 533.8 eV after annealing to ∼520 K. The latter cannot be straightforwardly assigned, but based on its binding energy it probably originates from oxygen-containing moieties decoupled from the metal surface and distinct from either phenol or phenolate.[31] It gives evidence of further thermally induced alterations, and accordingly its contribution increases at higher temperatures. The corresponding carbon signatures in the XP and NEXAFS spectra (Supporting Information Figure S2e) are unchanged, supporting the conclusion that the carbon molecular backbone remains mostly intact upon the temperature-induced transformation.

After annealing to 700 K, the ratio of the O 1s to C 1s signal decreases by approximately 65%, indicating significant loss of oxygen, while concomitantly the intensity of the signal at 533.8 eV roughly doubles (Figure 5e). The carbon signatures for both the C 1s XPS and K-edge NEXAFS (Supporting Information Figure S2f) corroborate remarkable changes in the molecular structure, with loss of the phenolate and methyl signatures. The high annealing temperature of formation and the modified appearance of the molecular chains of type B in the STM images (Figure 3b) point to covalently linked carbonaceous species. The C 1s signal intensities in the XP spectra show that the molecular coverage remains approximately constant until this final annealing step, upon which the intensity decreases significantly due to a loss of molecular fragments. For comparison, thermal dissociation of BPA polycarbonate at 730 K results in a variety of aliphatic and aromatic carbon fragments including phenol and substituted phenol moieties.[14] However, all of these small fragments would desorb from the surface in the course of the annealing procedure.

NEXAFS measurements as a function of the photon incidence angle indicate that the average tilt angle of the combined contribution of the two phenol rings lies between 30° and 40° (Supporting Information Figures S2 and S3) with respect to the copper surface plane. This average tilt angle extracted by comparison with the theoretically predicted curves does not vary as a function of temperature. As the resonance energy of the two phenol rings is the same, the deduced tilt angle must be considered as having contributions from both rings. Taking into account that the accuracy of NEXAFS is ~10°; this allows a broad variety of different combinations of tilt angles of the individual phenol groups in a single BPA molecule ranging from 0°/80° to 30°/30°. The window of possible adsorption geometries consistent with the NEXAFS measurements may increase even further, if molecules in different adsorption geometries coexist on the surface; nonetheless the analysis rules out in a definitive way a conformation with both rings either parallel or perpendicular to the surface.

Molecular Modeling. Combined information from STM, X-ray spectroscopy and DFT studies allow us to derive molecular models for the network-, dimer-, and trimer-phases. Although catalytically active Cu adatoms might be active sites in the deprotonation process,[32] the intermolecular distances measured from the STM images do not suggest their incorporation in the supramolecular assembly, *i.e.*, metal−organic complexes do not form. Additionally there is no evidence of the perturbation of the step arising from detachment of adatoms. Alcohol groups in close proximity to the copper substrate are expected to readily deprotonate at the deposition temperature of 260 K.[26,33] In the present case, 25% (dimer- and trimer-phases) to 60% (network-phase) of the oxygen signal corresponds to

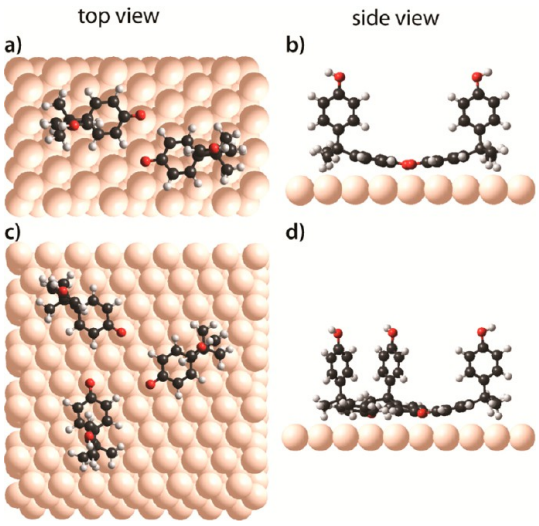

Figure 6. DFT-optimized geometries of (a, b) the dimeric motif and (c, d) the trimeric motif of the BPA binding configurations on Cu(111) in top view (a, c) and side view (b, d). C, O, H, and Cu atoms are shown in black, red, white, and orange, respectively.

intact phenol, suggesting that some of these groups are protected from the metallic surface. Taking into account the angular dependence of the NEXAFS measurements, a possible adsorption conformation of the molecule is one with a phenol ring standing up and the other being close to parallel to the surface, which is consistent with the tilt angles between 0° and 25° that have been reported for phenol adsorbed on surfaces such as Cu(110),[30] Pt(111),[34] and Ni(111).[35] Indeed, DFT modeling identified a local energy minimum for such an adsorption geometry, which is illustrated in Figure 1b. Although the calculations indicate a flat, distorted BPA configuration with even lower energy (see Supporting Information Figure S5), its geometrical footprint contradicts the determined intermolecular distances in the dimer and trimer motifs. Accordingly, the adsorption geometry of the monomer in Figure 1b was chosen as the basis to compute models for both observed binding motifs (Figure 6). The trimer motif can be built up from three molecules, each rotated by ±120°. The flat-lying phenol rings of all BPA molecules are deprotonated due to the contact with the copper surface, allowing intermolecular ═CH···O$^-$ hydrogen bonding[36] (Figure 6c,d). CH···O type bonding schemes have been identified previously in protein−protein interactions,[37] but with the involvement of organic ring systems they have been associated with noncovalent interactions distinct from H-bonds.[38] Nevertheless, in the presence of ionic proton acceptors, formation of ═CH···O$^-$ hydrogen bonds is likely.

Notably the self-assembly must also be dictated to a certain extent by the interaction with the substrate: the DFT calculations show that BPA units within the dimer (and the trimer) bonding motif retain the same adsorption geometry with respect to the Cu(111) surface, with

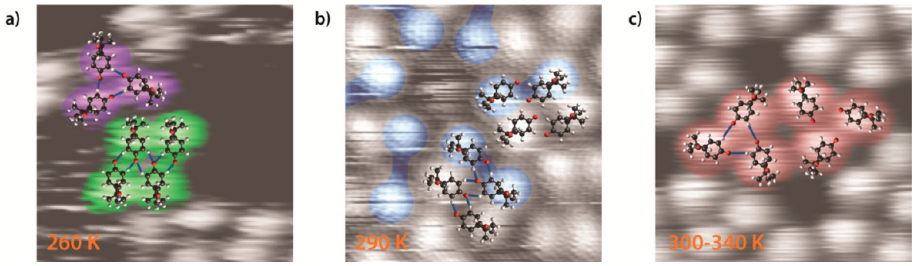

Figure 7. Proposed ball-and-stick models for BPA structures on Cu(111) overlaid on STM images: (a) Network-phase with trimeric and dimeric motifs, (b) dimer-phase, and (c) trimer-phase. C, O, and H atoms are shown in black, red, and white, respectively. The temperatures indicate the thermal treatment after which these phases of BPA form on Cu(111).

the oxygen atom of the flat-lying BPA phenolate located close to the atop site. This finding is corroborated by the absence of any moiré pattern in either the dimer- or the trimer-phases.

The network-phase consists of trimers and dimers connected *via* the flat-lying phenolates. The packing suggests that the dimer and the trimer binding motifs are stabilized by hydrogen bonds between the flat-lying rings (Figure 7a). Similar H-bond motifs exist in surface-confined carboxylate layers.[39−42] For the dimer within the network phase, the DFT calculation matches closely the STM images, whereas for the trimer the intermolecular distances were found to be somewhat shorter.

In the following we focus on the phases with a higher degree of deprotonation. The acute reader might have noticed that although every other molecule appears dimmer in the STM images of the dimer-phase (in good agreement with the XPS showing molecules in different oxidation states), this asymmetry is not observed for the trimer-phase. As the XPS core levels and the NEXAFS do not change in the temperature range covering the transition between the dimer- and the trimer-phases, we deduce that the chemical composition of the two phases is very similar. The ratio of phenol to phenolate signal indicates that in the trimer-phase there is still a significant percentage of molecules retaining an intact phenol group. Furthermore the temperature required for all phenol groups to deprotonate is more than 80 K higher than the highest annealing temperature after which the trimer-phase is observed. Therefore we will not address the exact degree of deprotonation within the proposed bonding scheme, but we emphasize that the spectroscopic study shows a mixture of standing-up phenols and phenolates in the molecular ensembles of the dimer- and trimer-phases.

The assembly of the dimer-phase suggests the expression of cooperative interactions, namely, $O^{-}\cdots H-C$ hydrogen bonding between the flat-lying phenols. $O-H\cdots O^{-}$ interactions between the two upright hydroxyl groups might moreover play an additional role in the network stability,[40] especially if one of the neighboring alcohol groups is deprotonated. The structure can be described in terms of pairs of dimers, resulting in a zigzag arrangement of hydrogen bonds (indicated by blue lines in Figure 7b). Similarly, the close-packed assembly of the trimer-phase can be described accurately by the trimer binding motif shown in Figure 6c,d, with the hydroxy group of all flat-lying rings deprotonated. The hydrogen bonds in this case are arranged in a cyclic fashion (indicated by blue lines in Figure 7c). Furthermore, we may envisage attractive interactions between standing up phenols of neighboring trimers, which are not included in our calculations. Note that the transition between the dimer- and the trimer-phase does not seem to be driven by a chemical transformation. Thus, we assume that the interaction with the substrate mediates the changes observed in STM. Indeed, we find that BPA molecules in the DFT model of the trimer are closer to the adsorption site calculated for a BPA monomer in comparison to the DFT model of the BPA molecules in the dimer.

SUMMARY AND CONCLUSIONS

Our multitechnique experimental study to characterize the evolution of bisphenol A on Cu(111) as a function of the annealing temperature revealed an intriguing diversity of configurations of the molecular overlayer. For the network-phase approximately 50% of the phenol groups are deprotonated, consistently with a conformation of the molecule in which part of the phenol groups are protected against adsorption-induced deprotonation at ∼260 K by tilting away from the surface. The phenolate signal percentage increases to ∼75% for the dimer-phase and the trimer-phase, evidencing a temperature-induced stepwise deprotonation. Supported by DFT calculations, models for the three ordered phases were proposed consisting of BPA molecules with one phenol ring being nearly parallel to the copper surface and the other one pointing away from the surface. The self-assembly is mediated by intermolecular hydrogen bonding and was found to be in registry with the Cu(111) substrate.

The chemical state with all the phenols tilted toward the surface and approximately half of the standing up phenols being deprotonated exhibit a particular stability, as it requires heating to 400 K to further deprotonate the BPA molecules.

Chains built up by linked molecular modules (type A) are observed in the STM micrographs after heating to 470 K, whereas the XPS study shows a complete conversion to phenolate at this temperature. The spectroscopic signatures of the carbon atoms suggest that the BPA component within these chains retains its carbon backbone intact. Further annealing to temperatures higher than 570 K causes the chains to reshape into type B, which exhibits an ill-defined carbonaceous composition.

These results reveal that BPA molecules show appreciable substrate anchoring. This robustness enables the observation of a remarkable sequence of thermally activated chemical transformations within the molecular layer and hints toward a rich and hard to predict chemistry in biological environments as well.

METHODS

Sample Preparation. The clean, atomically flat surface of the Cu(111) single-crystal surface was prepared *in vacuo* by repeated cycles of Ar^+ sputtering and annealing at 770 K. BPA molecules (Sigma Aldrich, purity >99%) were deposited onto Cu(111) from a quartz crucible by sublimation at ~400 K. Before deposition, the sample was cooled to a temperature of approximately 260 K. The successful sublimation of the intact molecules was confirmed by the XPS signatures of C 1s and O 1s corresponding to a BPA multilayer (Supporting Information Figure S6).

STM. The STM experiments were carried out in a custom-designed ultra-high-vacuum system operating at a base pressure of $\sim 4 \times 10^{-10}$ mbar and equipped with a commercially available variable-temperature STM (type Specs "Aarhus 150").[43] All STM measurements were performed at a sample temperature of 180−220 K with a chemically etched W tip at room temperature. U_t refers to the bias applied to the sample. The images were processed with the WSxM software.[44]

Synchrotron Light Measurements. X-ray spectroscopy measurements were performed at the HE-SGM dipole beamline at BESSY II in Berlin in normal emission. The excitation energies for the acquisition of the O 1s and C 1s XP spectral regions were 680 and 435 eV, respectively. The binding energy scale was calibrated against the Cu $3p_{3/2}$ core level at 75.1 eV.[45] XP spectra were fitted with Voigt functions after subtraction of a linear or Shirley[46] background from the O 1s and C 1s spectra, respectively. X-ray spectroscopy measurements were performed at sample temperatures of 130−140 K. XPS and NEXAFS measurements of a freshly prepared surface and after some hours of measuring were consistent, thus excluding artifacts due to beam damage.

Modeling. As the exchange−correlation functional for the DFT calculations we employed the revPBE[47] generalized-gradient approximation, with long-range dispersion included using the DFT-D3 empirical correction.[48] We described the surface with the adsorbate in the slab geometry in an orthorhombic cell with unit cell dimension $12.763 \times 22.107 \times 35$ Å^3 (monomer and dimer) or $25.527 \times 22.107 \times 35$ Å^3 (trimer), where the experimental lattice constant 3.61 Å was used and the substrate consisted of four layers of Cu. The two topmost layers of substrate and the adsorbates were fully relaxed.

The Kohn−Sham equations were solved within the Gaussian plane wave (GPW) scheme[49] implemented in the QuickStep module[50] in the CP2K (http://www.CP2K.org/) suite. The details are similar to our recent investigations of h-BN adsorbed on a transition metal surface:[51] The ionic cores were described using Goedecker−Teter−Hutter pseudopotentials,[52] the density was expanded in a plane wave basis set up to the cutoff energy of 500 Ry, and the wave functions in the DZVP Gaussian basis set were MOLOPT type.[53] Only the Γ-point was used to sample the surface Brillouin zone, and Fermi−Dirac broadening at 300 K was used to broaden the occupation numbers around the Fermi energy.

Conflict of Interest: The authors declare no competing financial interest.

Supporting Information Available: STM images showing the mirror phases of the dimer- and the trimer-phase, NEXAFS C K-edge spectra, quantitative analysis and experimental details, an alternative DFT geometry of the BPA monomer, and O 1s and C 1s of multilayer BPA film on Cu(111). This material is available free of charge *via* the Internet at http://pubs.acs.org.

Acknowledgment. This work was supported by the ERC Advanced Grant MolArt (no. 247299). A.C.P. acknowledges a Marie Curie Intra-European Fellowship for Career Development (project NASUMECA, no. 274842). APS thanks CSCS (Centro Svizzero di Calcolo Scientifico, project s425). We thank Helmholtz-Zentrum Berlin (HZB) for the allocation of synchrotron radiation beamtime and financial support. Dr. A. Nefedov and Prof. Ch. Wöll are gratefully acknowledged for providing access to the HE-SGM end station.

REFERENCES AND NOTES

1. Meeker, J. D.; Ehrlich, S.; Toth, T. L.; Wright, D. L.; Calafat, A. M.; Trisini, A. T.; Ye, X.; Hauser, R. Semen Quality and Sperm DNA Damage in Relation to Urinary Bisphenol A among Men from an Infertility Clinic. *Reprod. Toxicol.* **2010**, *30*, 532–539.
2. Tharp, A. P.; Maffini, M. V.; Hunt, P. A.; VandeVoort, C. A.; Sonnenschein, C.; Soto, A. M. Bisphenol A Alters the Development of the Rhesus Monkey Mammary Gland. *Proc. Natl. Acad. Sci. U.S.A.* **2012**, *109*, 8190–8195.
3. Dolinoy, D. C.; Huang, D.; Jirtle, R. L. Maternal Nutrient Supplementation Counteracts Bisphenol A-Induced DNA Hypomethylation in Early Development. *Proc. Natl. Acad. Sci. U.S.A.* **2007**, *104*, 13056–13061.
4. Bromer, J. G.; Zhou, Y.; Taylor, M. B.; Doherty, L.; Taylor, H. S. Bisphenol-A Exposure in Utero Leads to Epigenetic Alterations in the Developmental Programming of Uterine Estrogen Response. *FASEB J.* **2010**, *24*, 2273–2280.
5. Fischer, S.; Papageorgiou, A. C.; Marschall, M.; Reichert, J.; Diller, K.; Klappenberger, F.; Allegretti, F.; Nefedov, A.; Wöll, Ch.; Barth, J. V. l-Cysteine on Ag(111): A Combined STM and X-ray Spectroscopy Study of Anchorage and Deprotonation. *J. Phys. Chem. C* **2012**, *116*, 20356–20362.
6. Papageorgiou, A. C.; Fischer, S.; Reichert, J.; Diller, K.; Blobner, F.; Klappenberger, F.; Allegretti, F.; Seitsonen, A. P.; Barth, J. V. Chemical Transformations Drive Complex Self-Assembly of Uracil on Close-Packed Coinage Metal Surfaces. *ACS Nano* **2012**, *6*, 2477–2486.
7. Schiffrin, A.; Reichert, J.; Pennec, Y.; Auwärter, W.; Weber-Bargioni, A.; Marschall, M.; Dell'Angela, M.; Cvetko, D.; Bavdek, G.; Cossaro, A.; *et al.* Self-Assembly of l-Methionine on Cu(111): Steering Chiral Organization by Substrate Reactivity and Thermal Activation. *J. Phys. Chem. C* **2009**, *113*, 12101–12108.
8. Kühnle, A. Self-Assembly of Organic Molecules at Metal Surfaces. *Curr. Opin. Colloid Interface Sci.* **2009**, *14*, 157–168.
9. Irvin, J. A.; Neef, C. J.; Kane, K. M.; Cassidy, P. E.; Tullos, G.; St. Clair, A. K. Polyethers Derived From Bisphenols and Highly Fluorinated Aromatics. *J. Polym. Sci., Part A: Polym. Chem.* **1992**, *30*, 1675–1679.
10. Uyama, H.; Maruichi, N.; Tonami, H.; Kobayashi, S. Peroxidase-Catalyzed Oxidative Polymerization of Bisphenols. *Biomacromolecules* **2001**, *3*, 187–193.
11. Muir, B. W.; Mc Arthur, S. L.; Thissen, H.; Simon, G. P.; Griesser, H. J.; Castner, D. G. Effects of Oxygen Plasma

Treatment on the Surface of Bisphenol A Polycarbonate: A Study Using SIMS, Principal Component Analysis, Ellipsometry, XPS and AFM Nanoindentation. *Surf. Interface Anal.* **2006**, *38*, 1186–1197.
12. Mercier, J. P.; Aklonis, J. J.; Litt, M.; Tobolsky, A. V. Viscoelastic Behavior of the Polycarbonate of Bisphenol A. *J. Appl. Polym. Sci.* **1965**, *9*, 447–459.
13. Rivaton, A. Recent Advances in Bisphenol-A Polycarbonate Photodegradation. *Polym. Degrad. Stab.* **1995**, *49*, 163–179.
14. McNeill, I. C.; Rincon, A. Degradation Studies of Some Polyesters and Polycarbonates—8. Bisphenol A Polycarbonate. *Polym. Degrad. Stab.* **1991**, *31*, 163–180.
15. Iski, E. V.; Johnston, B. F.; Florence, A. J.; Urquhart, A. J.; Sykes, E. C. H. Surface-Mediated Two-Dimensional Growth of the Pharmaceutical Carbamazepine. *ACS Nano* **2010**, *4*, 5061–5068.
16. Kalashnyk, N.; Nielsen, J. T.; Nielsen, E. H.; Skrydstrup, T.; Otzen, D. E.; Lægsgaard, E.; Wang, C.; Besenbacher, F.; Nielsen, N. C.; Linderoth, T. R. Scanning Tunneling Microscopy Reveals Single-Molecule Insights into the Self-Assembly of Amyloid Fibrils. *ACS Nano* **2012**, *6*, 6882–6889.
17. Jewell, A. D.; Sykes, E. C. H.; Kyriakou, G. Molecular-Scale Surface Chemistry of a Common Metal Nanoparticle Capping Agent: Triphenylphosphine on Au(111). *ACS Nano* **2012**, *6*, 3545–3552.
18. Grillo, F.; Mugnaini, V.; Oliveros, M.; Francis, S. M.; Choi, D.-J.; Rastei, M. V.; Limot, L.; Cepek, C.; Pedio, M.; Bromley, S. T.; *et al*. Chiral Conformation at a Molecular Level of a Propeller-Like Open-Shell Molecule on Au(111). *J. Phys. Chem. Lett.* **2012**, *3*, 1559–1564.
19. Cossaro, A.; Terreni, S.; Cavalleri, O.; Prato, M.; Cvetko, D.; Morgante, A.; Floreano, L.; Canepa, M. Electronic and Geometric Characterization of the l-Cysteine Paired-Row Phase on Au(110). *Langmuir* **2006**, *22*, 11193–11198.
20. Reichert, J.; Schiffrin, A.; Auwärter, W.; Weber-Bargioni, A.; Marschall, M.; Dell'Angela, M.; Cvetko, D.; Bavdek, G.; Cossaro, A.; Morgante, A.; *et al*. l-Tyrosine on Ag(111): Universality of the Amino Acid 2D Zwitterionic Bonding Scheme? *ACS Nano* **2010**, *4*, 1218–1226.
21. McArthur, S. L. Applications of XPS in Bioengineering. *Surf. Interface Anal.* **2006**, *38*, 1380–1385.
22. Klappenberger, F. Two-Dimensional Functional Molecular Nanoarchitectures – Complementary Investigations with Scanning Tunneling Microscopy and X-Ray Spectroscopy. *Prog. Surf. Sci.* **2014**, *89*, 1–55.
23. Blüm, M.-C.; Ćavar, E.; Pivetta, M.; Patthey, F.; Schneider, W.-D. Conservation of Chirality in a Hierarchical Supramolecular Self-Assembled Structure with Pentagonal Symmetry. *Angew. Chem., Int. Ed.* **2005**, *44*, 5334–5337.
24. Spillmann, H.; Dmitriev, A.; Lin, N.; Messina, P.; Barth, J. V.; Kern, K. Hierarchical Assembly of Two-Dimensional Homochiral Nanocavity Arrays. *J. Am. Chem. Soc.* **2003**, *125*, 10725–10728.
25. Bowker, M.; Madix, R. J. XPS, UPS and Thermal Desorption Studies of Alcohol Adsorption on Cu(110): I. Methanol. *Surf. Sci.* **1980**, *95*, 190–206.
26. Bowker, M.; Madix, R. J. XPS, UPS and Thermal Desorption Studies of Alcohol Adsorption on Cu(110): II. Higher Alcohols. *Surf. Sci.* **1982**, *116*, 549–572.
27. del Olmo, M.; Zafra, A.; Gonzalez-Casado, A.; Vilchez, J. L. The Use of b-Cyclodextrin Inclusion Complexes for the Analysis of Bisphenol A Residues in Water by Spectrofluorimetry. *Int. J. Environ. Anal. Chem.* **1998**, *69*, 99–110.
28. Spitzer, A.; Lüth, H. An XPS Study of the Water Adsorption on Cu(110). *Surf. Sci.* **1985**, *160*, 353–361.
29. Norton, P. R.; Tapping, R. L.; Goodale, J. W. High Resolution Photoemission Study of the Physisorption and Chemisorption of CO on Copper and Gold. *Surf. Sci.* **1978**, *72*, 33–44.
30. Richardson, N. V.; Hofmann, P. A Spectroscopic Investigation of the Adsorption of Phenol on Cu{110}. *Vacuum* **1983**, *33*, 793–796.
31. Beamson, G.; Briggs, D. *High Resolution XPS of Organic Polymers: The Scienta ESCA300 Database*; Wiley: New York, 1992.
32. Lin, N.; Payer, D.; Dmitriev, A.; Strunskus, T.; Wöll, Ch.; Barth, J. V.; Kern, K. Two-Dimensional Adatom Gas Bestowing Dynamic Heterogeneity on Surfaces. *Angew. Chem., Int. Ed.* **2005**, *44*, 1488–1491.
33. Guo, X.-C.; Madix, R. J. Monolayer Structure of Phenoxy Species on Cu(110): An STM Study. *Surf. Sci.* **1995**, *341*, L1065–L1071.
34. Ihm, H.; White, J. M. Stepwise Dissociation of Thermally Activated Phenol on Pt(111). *J. Phys. Chem. B* **2000**, *104*, 6202–6211.
35. Myers, A. K.; Benziger, J. B. Effect of Substituent Groups on the Interaction of Benzene with Nickel(111). *Langmuir* **1989**, *5*, 1270–1288.
36. Arunan, E.; Desiraju, G. R.; Klein, R. A.; Sadlej, J.; Scheiner, S.; Alkorta, I.; Clary, D. C.; Carbtree, R. H.; Dannenberg, J. J.; Hobza, P.; *et al*. Definition of the Hydrogen Bond (IUPAC Recommendations 2011). *Pure Appl. Chem.* **2011**, *83*, 1637–1641.
37. Jiang, L.; Lai, L. CH···O Hydrogen Bonds at Protein-Protein Interfaces. *J. Biol. Chem.* **2002**, *277*, 37732–37740.
38. Arras, E.; Seitsonen, A. P.; Klappenberger, F.; Barth, J. V. Nature of the Attractive Interaction between Proton Acceptors and Organic Ring Systems. *Phys. Chem. Chem. Phys.* **2012**, *14*, 15995–16001.
39. Stepanow, S.; Lin, N.; Vidal, F.; Landa, A.; Ruben, M.; Barth, J. V.; Kern, K. Programming Supramolecular Assembly and Chirality in Two-Dimensional Dicarboxylate Networks on a Cu(100) Surface. *Nano Lett.* **2005**, *5*, 901–904.
40. Dmitriev, A.; Spillmann, H.; Stepanow, S.; Strunskus, T.; Wöll, Ch.; Seitsonen, A. P.; Lingenfelder, M.; Lin, N.; Barth, J. V.; Kern, K. Asymmetry Induction by Cooperative Intermolecular Hydrogen Bonds in Surface-Anchored Layers of Achiral Molecules. *ChemPhysChem* **2006**, *7*, 2197–2204.
41. Payer, D.; Comisso, A.; Dmitriev, A.; Strunskus, T.; Lin, N.; Wöll, Ch.; DeVita, A.; Barth, J. V.; Kern, K. Ionic Hydrogen Bonds Controlling Two-Dimensional Supramolecular Systems at a Metal Surface. *Chem.—Eur. J.* **2007**, *13*, 3900–3906.
42. Cañas-Ventura, M. E.; Klappenberger, F.; Clair, S.; Pons, S.; Kern, K.; Brune, H.; Strunskus, T.; Wöll, Ch.; Fasel, R.; Barth, J. V. Coexistence of One- and Two-Dimensional Supramolecular Assemblies of Terephthalic Acid on Pd(111) Due to Self-Limiting Deprotonation. *J. Chem. Phys.* **2006**, *125*, 184710.
43. Besenbacher, F.; Lægsgaard, E.; Stensgaard, I. Fast-Scanning STM Studies. *Mater. Today* **2005**, *8*, 26–30.
44. Horcas, I.; Fernandez, R.; Gomez-Rodriguez, J. M.; Colchero, J.; Gomez-Herrero, J.; Baro, A. M. WSXM: A Software for Scanning Probe Microscopy and a Tool for Nanotechnology. *Rev. Sci. Instrum.* **2007**, *78*, 013705.
45. Fuggle, J. C.; Mårtensson, N. Core-Level Binding Energies in Metals. *J. Electron Spectrosc. Relat. Phenom.* **1980**, *21*, 275–281.
46. Shirley, D. A. High-Resolution X-Ray Photoemission Spectrum of the Valence Bands of Gold. *Phys. Rev. B* **1972**, *5*, 4709–4714.
47. Zhang, Y.; Yang, W. Comment on "Generalized Gradient Approximation Made Simple". *Phys. Rev. Lett.* **1998**, *80*, 890.
48. Grimme, S.; Antony, J.; Ehrlich, S.; Krieg, H. A Consistent and Accurate Ab Initio Parametrization of Density Functional Dispersion Correction (DFT-D) for the 94 Elements H-Pu. *J. Chem. Phys.* **2010**, *132*, 154104.
49. Lippert, G.; Hutter, J.; Parrinello, M. Michele A Hybrid Gaussian and Plane Wave Density Functional Scheme. *Mol. Phys.* **1997**, *92*, 477–488.
50. VandeVondele, J.; Krack, M.; Mohamed, F.; Parrinello, M.; Chassaing, T.; Hutter, J. Quickstep: Fast and Accurate Density Functional Calculations Using a Mixed Gaussian and Plane Waves Approach. *Comput. Phys. Commun.* **2005**, *167*, 103–128.

51. Gómez Díaz, J.; Ding, Y.; Koitz, R.; Seitsonen, A.; Iannuzzi, M.; Hutter, J. Hexagonal Boron Nitride on Transition Metal Surfaces. *Theor. Chem. Acc.* **2013**, *132*, 1350.
52. Goedecker, S.; Teter, M.; Hutter, J. Separable Dual-Space Gaussian Pseudopotentials. *Phys. Rev. B* **1996**, *54*, 1703–1710.
53. VandeVondele, J.; Hutter, J. Gaussian Basis Sets for Accurate Calculations on Molecular Systems in Gas and Condensed Phases. *J. Chem. Phys.* **2007**, *127*, 114105.